# Local Hydrodynamics Modeling of a Gas–Liquid–Solid Three-Phase Bubble Column

**Xiaoqiang Jia, Jianping Wen, Haoli Zhou, Wei Feng, and Qing Yuan**
Dept. of Biochemical Engineering, School of Chemical Engineering and Technology, Tianjin University, Tianjin 300072, China

*DOI 10.1002/aic.11254*
*Published online July 25, 2007 in Wiley InterScience (www.interscience.wiley.com).*

*A three-dimensional (3D) transient model was developed to simulate the local hydrodynamics of a gas–liquid–solid three-phase bubble column using the computational fluid dynamic method, where the multiple size group model was adopted to determine the size distribution of the gas bubbles. Model simulation results, such as the local time-averaged gas holdups and axial liquid velocities, were validated by experimental measurements under varied operating conditions, e.g., superficial gas velocities and initial solid loadings at different locations in the three-phase bubble column. Furthermore, the local transient hydrodynamic characteristics, such as gas holdups, liquid velocities, and solid holdups, as well as gas bubble size distribution were predicted reasonably by the developed model for the dynamic behaviors of the three-phase bubble column.* © 2007 American Institute of Chemical Engineers *AIChE J,* 53: 2221–2231, 2007

*Keywords: three-phase, bubble column, local hydrodynamics, modeling, MUSIG*

## Introduction

Bubble columns are widely used as multiphase contactors for carrying out gas–liquid–solid three-phase reactions in a variety of industrial applications, especially in biochemical reaction engineering where microorganisms are immobilized to solid carriers to manufacture valuable bioproducts.[1] The dispersion and interfacial heat- and mass-transfer fluxes, as well as the biochemical reaction rates, are closely related to the fluid dynamics of the system through the liquid–gas as well as liquid–solid contact area and the turbulence properties of the flow. Thus there is considerable interest, within both academia and industry, to improve the limited understanding of the complex multiphase flow phenomena involved, which prevents optimal design and scaleup of the bubble columns.[2]

Computational fluid dynamic (CFD) method has been promoted as a useful tool for understanding bubble column flow behaviors in the last decade, which to a large extent can replace the time-consuming and expensive experiments.[3] Two main approaches exist, i.e., the Eulerian approach, which regards the dispersed phases as interpenetrating continua, and the Lagrangian approach, which regards the dispersed phases as discrete entities.[4–6] Both methods can lead to the same results if adequate numerical methods are used to solve the resulting equations.[7] However, since the Lagrangian approach needs tremendous computational effort for tracking every single gas bubble and/or solid particle, it is mainly used in very dilute systems or for special applications like residence time distribution calculations.[8]

Although past studies often considered the gas bubbles to be uniformly distributed in bubble columns, numerical predictions of multiphase flow behaviors nowadays have to take into account the evolution of bubble size distribution and bubble–bubble interactions, which play very significant roles in calculation of the gas–liquid specific interfacial area.[9–14] With the so-called multiple size group (MUSIG) model, the bubble sizes come directly from the population balance equation, and the bubble–bubble interactions are controlled by bubble coalescence and breakup laws.[15,16]

Correspondence concerning this article should be addressed to J. P. Wen at jpwen@tju.edu.cn.

Several authors have reported on attempts at solving the two-dimensional (2D) multiphase flow but only found that no reasonable, grid-independent results could be obtained; the same outcome is reported on steady-state calculations,[17–20] thus making 3D transient calculations unavoidable in reasonably modeling of the multiphase flow.[21–23]

Still, most literatures hitherto are limited to two-phase flows.[24–31] Reports of modeling on gas–liquid–solid three-phase flows in bubble columns are rather limited. Michele and Hempel developed a gas–liquid–solid three-phase CFD model, which can correctly reproduce the fluidization behavior of the bubble column with implementing the direct interactions of dispersed gas and solid phases.[32] However, fitting parameters and a uniform bubble diameter had to be used in the calculations; moreover the integral gas holdup prediction could not account for the flow regimes and the axial liquid velocities were systematically underestimated. Glover and Generalis presented a 2D mixture model for simulating the gas–liquid–solid flows in a 5:1 aspect ratio bubble column without considering the interphase forces, and a uniform bubble diameter was used.[33] Contours of the mixture velocity vector, gas holdup and solid holdup were predicted by the model with a conclusion that the introduction of a solid phase transport did not disrupt the flow structure of the gas phase compared with the gas–liquid flow, although no experimental validation of the model was done. Zhang and Ahmadi used an Eulerian–Lagrangian model for simulation of gas–liquid–solid three-phase flow assuming that the bubbles remained spherical and their shape variations were neglected.[34] The predicted results were in good agreement with another author's experimental data and the transient flow characteristics of the three-phase flow were successfully captured. But this model only dealt with very small amount of bubbles and particles and the simulation time was just only 1 s, thus was hard to be utilized in real process modeling.

The objective of this study is to develop a 3D transient CFD model for simulating the local hydrodynamics of a gas–liquid–solid three-phase bubble column, with the bubble size distribution to be determined by the MUSIG model. The local time-averaged gas holdups and axial liquid velocities of the model simulation results are to be validated by the experimental measurements under varied operating conditions and at different locations in the bubble column. Furthermore, the local transient gas holdups, solid holdups, liquid velocities and bubble size distribution are to be predicted by the developed model.

## Experimental Setup

The experimental apparatus was the same as the one used by Feng et al. in our lab. The column had a square cross-section of 0.2 m × 0.2 m and a height of 1.2 m. A square stainless steel perforated distributor plate with the width of 50 mm contained 625 holes with the diameter of 0.5 mm, and was centrally located at the bottom of the column. The measurements of local gas holdups using the conductivity probes, local liquid velocities using the 3D Laser Doppler Anemometer (LDA) system were all following the same strategies.[35] Tap water was used as the liquid phase with a static height of 0.6 m. Air was used as the gas phase. Alginate gel beads were used as the solid phase to represent the immobilizing carriers in future multiphase bioreaction studies, which were prepared by extruding 2% (w/v) sodium alginate through a needle into a stirred solution of 0.1 M calcium chloride. The height of the needle and the rate of stirring of the calcium chloride solution were adjusted carefully so that uniform spherical gel beads were obtained with an average diameter of 3.5 mm. Beads were left to harden in the calcium chloride solution for 2 h for complete replacement of sodium ions by calcium ions. The apparent density was evaluated by putting a number of alginate gel beads in a 50-mL glass cylinder, and an average value of 1048 kg/m$^3$ was obtained. Superficial gas velocity was set to be 0.01, 0.02, 0.03 m/s to ensure that the measured local time-averaged gas holdups were lower than 20%, and the initial solid loadings were set to be 1, 2, 3% of the working volume of the reactor, as the application of the LDA technology operated in backscatter mode in multiphase flows was limited to a low gas holdup (<20%) and a low solid loading (<4%), according to the work done by Cui and Fan.[36]

## Model Development

### *Governing equations*

In this work, a 3D transient CFD model is developed to simulate the local hydrodynamics of the gas–liquid–solid three-phase bubble column. Eulerian approach is adopted to describe the flow behavior of each phase. Water is considered to be the continuous phase, whereas gas bubbles and solid particles are considered to be the dispersed phases.

The phase volume fractions satisfy the compatibility condition:

$$\alpha_g + \alpha_l + \alpha_s = 1 \tag{1}$$

The continuity balance equation for each phase is:

$$\frac{\partial(\rho_g \alpha_g)}{\partial t} + \nabla(\rho_g \alpha_g \mathbf{u}_g) = 0 \tag{2}$$

$$\frac{\partial(\rho_l \alpha_l)}{\partial t} + \nabla(\rho_l \alpha_l \mathbf{u}_l) = 0 \tag{3}$$

$$\frac{\partial(\rho_s \alpha_s)}{\partial t} + \nabla(\rho_s \alpha_s \mathbf{u}_s) = 0 \tag{4}$$

where $\rho$ is the density, $\alpha$ is the volume fraction, and $\mathbf{u}$ is the velocity vector of each phase.

The momentum balance equation for each phase is:

$$\frac{\partial(\rho_g \alpha_g \mathbf{u}_g)}{\partial t} + \nabla(\rho_g \alpha_g \mathbf{u}_g \mathbf{u}_g) = -\alpha_g \nabla p + \nabla\left(\alpha_g \mu_{\text{eff},g}\left(\nabla \mathbf{u}_g + \left(\nabla \mathbf{u}_g\right)^T\right)\right) + \rho_g \alpha_g \mathbf{g} - \mathbf{M}_{\text{I,lg}} \tag{5}$$

$$\frac{\partial(\rho_l \alpha_l \mathbf{u}_l)}{\partial t} + \nabla(\rho_l \alpha_l \mathbf{u}_l \mathbf{u}_l) = -\alpha_l \nabla p + \nabla\left(\alpha_l \mu_{\text{eff},l}\left(\nabla \mathbf{u}_l + \left(\nabla \mathbf{u}_l\right)^T\right)\right) + \rho_l \alpha_l \mathbf{g} + \mathbf{M}_{\text{I,lg}} + \mathbf{M}_{\text{I,ls}} \tag{6}$$

$$\frac{\partial(\rho_s \alpha_s \mathbf{u}_s)}{\partial t} + \nabla(\rho_s \alpha_s \mathbf{u}_s \mathbf{u}_s) = -\alpha_s \nabla p + \nabla\left(\alpha_s \mu_{\text{eff},s}\left(\nabla \mathbf{u}_s + \left(\nabla \mathbf{u}_s\right)^T\right)\right) + \rho_s \alpha_s \mathbf{g} - \mathbf{M}_{\text{I,ls}} \tag{7}$$

where $p$ is the pressure, $\mu_{\text{eff}}$ is the effective viscosity, $\mathbf{g}$ is the gravitational acceleration, and $\mathbf{M}_{\text{I}}$ is the interphase momentum transfer force.

### *Interphase momentum transfer*

In this study, only drag force and lift force between the continuous phase and the dispersed phases are considered. The drag force exerted by the dispersed phase on the continuous phase is calculated as:

$$\mathbf{M}_{\text{D,lg}} = \frac{3}{4}\frac{C_{\text{D,lg}}}{d_{\text{g}}}\rho_{\text{l}}\alpha_{\text{g}}\left|\mathbf{u}_{\text{g}} - \mathbf{u}_{\text{l}}\right|(\mathbf{u}_{\text{g}} - \mathbf{u}_{\text{l}}) \tag{8}$$

$$\mathbf{M}_{\text{D,ls}} = \frac{3}{4}\frac{C_{\text{D,ls}}}{d_{\text{s}}}\rho_{\text{l}}\alpha_{\text{s}}\left|\mathbf{u}_{\text{s}} - \mathbf{u}_{\text{l}}\right|(\mathbf{u}_{\text{s}} - \mathbf{u}_{\text{l}}) \tag{9}$$

where $C_{\text{D}}$ is the drag coefficient and $d$ is the diameter.

The drag coefficient exerted by the gas phase on the liquid phase, $C_{\text{D,lg}}$, is obtained by the Ishii–Zuber drag model[37]:

$$C_{\text{D,lg}} = \max\left(\frac{24}{Re_{\text{m}}}(1 + 0.15\text{Re}_{\text{m}}^{0.687}), \min\left(\frac{2}{3}\text{Eo}^{0.5}E(\alpha_{\text{g}}), \frac{8}{3}(1-\alpha_{\text{g}})^2\right)\right) \tag{10}$$

where $Re_{\text{m}}$ is the mixture Reynolds number:

$$Re_{\text{m}} = \frac{\rho_{\text{l}}d_{\text{g}}\left|\mathbf{u}_{\text{g}} - \mathbf{u}_{\text{l}}\right|}{\mu_{\text{m}}} \tag{11}$$

$$\mu_{\text{m}} = \mu_{\text{l}}(1-\alpha_{\text{g}})^{-2.5\mu^*} \tag{12}$$

$$\mu^* = \frac{\mu_{\text{g}} + 0.4\mu_{\text{l}}}{\mu_{\text{g}} + \mu_{\text{l}}} \tag{13}$$

And Eo is the Eotvos number:

$$\text{Eo} = \frac{\text{g}(\rho_{\text{l}} - \rho_{\text{g}})d_{\text{g}}^2}{\sigma} \tag{14}$$

where $\sigma$ is the surface tension between water and air.

And $E(\alpha_{\text{g}})$ is the correction term:

$$E(\alpha_{\text{g}}) = \frac{1 + 17.67f(\alpha_{\text{g}})^{6/7}}{18.67f(\alpha_{\text{g}})} \tag{15}$$

$$f(\alpha_{\text{g}}) = \frac{\mu_{\text{l}}}{\mu_{\text{m}}}(1-\alpha_{\text{g}})^{0.5} \tag{16}$$

The drag coefficient exerted by the solid phase on the liquid phase, $C_{\text{D,ls}}$, is obtained by the Wen Yu drag model[38]:

$$C_{\text{D,ls}} = \alpha_{\text{s}}^{-1.65}\ \max\left(\frac{24}{Re'}\left(1 + 0.15(Re')^{0.687}\right), 0.44\right) \tag{17}$$

$$Re' = \alpha_{\text{s}}Re \tag{18}$$

$$Re = \frac{\rho_{\text{l}}d_{\text{s}}\left|\mathbf{u}_{\text{s}} - \mathbf{u}_{\text{l}}\right|}{\mu_{\text{l}}} \tag{19}$$

The lift force acting perpendicular to the direction of relative motion of the two phases is given by:

$$\mathbf{M}_{\text{L,lg}} = C_{\text{L}}\rho_{\text{l}}\alpha_{\text{g}}(\mathbf{u}_{\text{g}} - \mathbf{u}_{\text{l}})\times(\nabla\times\mathbf{u}_{\text{l}}) \tag{20}$$

$$\mathbf{M}_{\text{L,ls}} = C_{\text{L}}\rho_{\text{l}}\alpha_{\text{s}}(\mathbf{u}_{\text{s}} - \mathbf{u}_{\text{l}})\times(\nabla\times\mathbf{u}_{\text{l}}) \tag{21}$$

where $C_{\text{L}}$ is the lift coefficient, the value of which is 0.5.

The interphase momentum transfer between the two dispersed phases, as well as virtual mass force and turbulent dispersion force between the continuous phase and the dispersed phases are all neglected in this study, as adding of these forces can not bring any obvious refinement to the current simulation results, but only convergence difficulties. The effects of bubble–bubble and solid–solid interactions are considered in the calculations of the drag coefficients between the continuous phase and the dispersed phases, respectively.

### *Turbulence closure*

The eddy viscosity hypothesis is assumed to hold for each turbulent phase. Diffusion of momentum in each phase is governed by an effective viscosity:

$$\mu_{\text{eff,l}} = \mu_{\text{l}} + \mu_{\text{T,l}} + \mu_{\text{g,l}} + \mu_{\text{s,l}} \tag{22}$$

$$\mu_{\text{eff,g}} = \mu_{\text{g}} + \mu_{\text{T,g}} \tag{23}$$

$$\mu_{\text{eff,s}} = \mu_{\text{s}} + \mu_{\text{T,s}} \tag{24}$$

where $\mu$ is the molecular viscosity, $\mu_{\text{T}}$ is the turbulence induced viscosity, and $\mu_{\text{g,l}}$, $\mu_{\text{s,l}}$ are the particle (gas bubble and solid particle) induced viscosities of the liquid phase.

The turbulence viscosity of the continuous phase is obtained by the $k-\varepsilon$ model:

$$\mu_{\text{T,l}} = C_{\mu}\rho_{\text{l}}\left(\frac{k^2}{\varepsilon}\right) \tag{25}$$

The description of the standard $k-\varepsilon$ model is:

$$\frac{\partial(\rho_{\text{l}}k)}{\partial t} + \nabla(\rho_{\text{l}}\mathbf{u}_{\text{l}}k) = \nabla\left(\left(\mu_{\text{l}} + \frac{\mu_{\text{T,l}}}{\sigma_k}\right)\nabla k\right) + P_k - \rho_{\text{l}}\varepsilon \tag{26}$$

$$\frac{\partial(\rho_{\text{l}}\varepsilon)}{\partial t} + \nabla(\rho_{\text{l}}\mathbf{u}_{\text{l}}\varepsilon) = \nabla\left(\left(\mu_{\text{l}} + \frac{\mu_{\text{T,l}}}{\sigma_{\varepsilon}}\right)\nabla\varepsilon\right) + \frac{\varepsilon}{k}(C_{\varepsilon 1}P_k - C_{\varepsilon 2}\rho_{\text{l}}\varepsilon) \tag{27}$$

where $k$ is the turbulence kinetic energy, defined as the variance of the fluctuations in velocity ($\text{m}^2/\text{s}^2$) and $\varepsilon$ is the turbulence eddy dissipation, defined as the rate at which the velocity fluctuations dissipate ($\text{m}^2/\text{s}^3$). The turbulence production due to viscous forces $P_k$ is:

$$P_k = \mu_{\text{T,l}}\nabla\mathbf{u}_{\text{l}}(\nabla\mathbf{u}_{\text{l}} + \nabla\mathbf{u}_{\text{l}}^T) - \frac{2}{3}\nabla\mathbf{u}_{\text{l}}(3\mu_{\text{T,l}}\nabla\mathbf{u}_{\text{l}} + \rho_{\text{l}}k) \tag{28}$$

The additional particle induced eddy viscosities of the continuous phase $\mu_{\text{g,l}}$ and $\mu_{\text{s,l}}$ are[39]:

$$\mu_{\text{g,l}} = C_{\mu p}\rho_{\text{l}}\alpha_{\text{g}}d_{\text{g}}\left|\mathbf{u}_{\text{g}} - \mathbf{u}_{\text{l}}\right| \tag{29}$$

$$\mu_{\text{s,l}} = C_{\mu p}\rho_{\text{l}}\alpha_{\text{s}}d_{\text{s}}\left|\mathbf{u}_{\text{s}} - \mathbf{u}_{\text{l}}\right| \tag{30}$$

The turbulence viscosity of the dispersed phase is calculated using the zero equation model:

$$\mu_{T,g} = \frac{\rho_g}{\rho_l}\mu_{T,l} \tag{31}$$

$$\mu_{T,s} = \frac{\rho_s}{\rho_l}\mu_{T,l} \tag{32}$$

The values of the constants are the standard ones: $C_{\varepsilon 1} = 1.44$, $C_{\varepsilon 2} = 1.92$, $C_\mu = 0.09$, $C_{\mu p} = 0.6$, $\sigma_k = 1.0$, $\sigma_\varepsilon = 1.3$. The value of the molecular viscosity of solid phase is set to be the same as that of water, since its variations will not bring obvious changes to the simulation results.[40]

### *Bubble size distribution*

The bubble size distribution is determined using the MUSIG model, e.g., population balance model with coalescence and breakup effects.[41] This MUSIG model considers that several bubble classes with different diameters $d_j$ can be represented by an equivalent phase with the Sauter mean diameter $d_g$. In this study, 10 bubble classes with the diameters ranging from 1 to 15 mm are considered based on the equal diameter discretization. Population balance is written as:

$$\frac{\partial(\rho_g \alpha_g f_i)}{\partial t} + \nabla(\rho_g \alpha_g f_i \mathbf{u}_g) = S_i \tag{33}$$

where $S_i$ is the source term because of bubble coalescence and breakup; $f_i$ is defined as the $i$th group fraction, which has a relationship with the gas holdup as:

$$n_i v_i = \alpha_g f_i \tag{34}$$

where $n_i$ is the $i$th group number density and $v_i$ is the $i$th group volume.

The Sauter mean diameter can thus be written as:

$$\frac{1}{d_g} = \sum \frac{f_i}{d_i} \tag{35}$$

The source term $S_i$ for the $i$th group is given by:

$$S_i = B_{\text{breakup}} - D_{\text{breakup}} + B_{\text{coalescence}} - D_{\text{coalescence}} \tag{36}$$

The right hand of the earlier equation is the birth and death source because of bubble breakup and coalescence, respectively.

The net source because of breakup to the $i$th group is:

$$B_i = \rho_g \alpha_g \left( \sum_{j>i} B_{ji} f_j - f_i \sum_{j<i} B_{ij} \right) \tag{37}$$

where $B_{ij}$ is the specific breakup rate, at which bubbles of $i$th group break into bubbles of $j$th group. Note that the total source because of breakup is zero when summed over all size groups.

The breakup rate is assumed to be a function of the breakup fraction as follows:

$$B_{ij} = B'_{ij} \int_{f_{BV}} df_{BV} \tag{38}$$

where $f_{BV}$ is the breakup fraction:

$$f_{BV} = \frac{m_j}{m_i} \tag{39}$$

The mass of a particular group can be related to the diameter as:

$$m_i = \frac{\pi}{6}\rho_g d_i^3 \tag{40}$$

Luo and Svendsen developed a theoretical model for the bubble breakup in turbulent suspensions.[42] The model is based on the theory of isotropic turbulence and probability. The breakup rate of size $i$ into bubbles of size $j$ is:

$$B'_{ij} = C_B(1-\alpha_g)\left(\frac{\varepsilon}{d_i^2}\right)^{1/3} \int_{\xi_{\min}}^{1} \frac{(1+\xi)^2}{\xi^{11/3}} \times \exp\left(-\frac{12({f_{BV}}^{2/3} + (1-f_{BV})^{2/3} - 1)\sigma}{\beta\rho_l \varepsilon^{2/3} d_i^{5/3} \xi^{11/3}}\right) d\xi \tag{41}$$

where $\sigma$ is the surface tension, and $\xi$ is the dimensionless size of eddies in the inertial subrange of isotropic turbulence. The lower limit of the integration is given by:

$$\xi_{\min} = 11.4\frac{1}{d_i}\left(\frac{1}{\varepsilon}\nu_l^3\right)^{1/4} \tag{42}$$

where $\varepsilon$ is the liquid phase eddy dissipation rate, and $\nu$ is the kinematic viscosity. And the constants $C_B = 0.923$ and $\beta = 2$.

The net source to $i$th group because of coalescence is:

$$C_i = (\rho_g \alpha_g)^2 \left( \frac{1}{2} \sum_{j \le i} \sum_{k \le i} C_{jk} f_j f_k \frac{m_j + m_k}{m_j m_k} X_{jki} - \sum_j C_{ij} f_i f_j \frac{1}{m_j} \right) \tag{43}$$

where $C_{ij}$ is the specific coalescence rate between the $i$th and $j$th groups. $X_{jki}$ is the fraction of mass because of coalescence between the $j$th and $k$th groups, which goes into group $i$.

$$X_{jki} = \begin{cases} \dfrac{m_j + m_k - m_{j-1}}{m_i - m_{i-1}} & m_{i-1} < m_j + m_k < m_i \\ \dfrac{m_{i+1} - (m_j + m_k)}{m_{i+1} - m_i} & \text{if } m_i < m_j + m_k < m_{i+1} \\ 0 & \text{otherwise} \end{cases} \tag{44}$$

When summed over all size groups, the net source because of coalescence is zero provided that $C_{ij} = C_{ji}$ and $\sum_i X_{jki} = 1$.

Prince and Blanch assumed that the coalescence of two bubbles occurs in three steps.[43] First, the bubbles collide trapping a small amount of liquid between them; this liquid film then drains until the liquid film separating the bubbles reaches a critical thickness; the film then ruptures and the bubbles join together. The coalescence process is therefore modeled by a collision rate of two bubbles and a collision efficiency relating to the times required for coalescence. And in the current implementation, only turbulent contributions

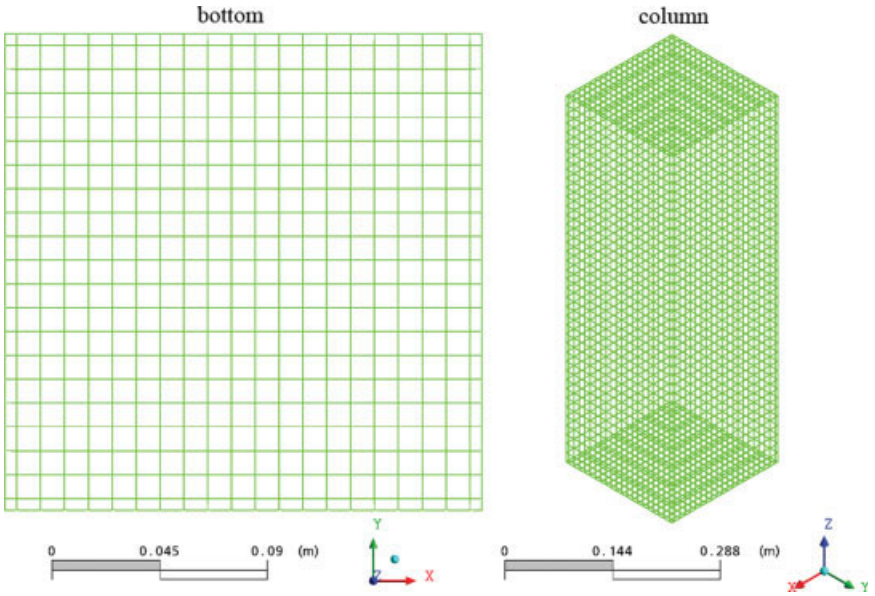


**Figure 1. Mesh partition of the bottom and the column of the reactor.**

[Color figure can be viewed in the online issue, which is available at www.interscience.wiley.com.]

are included in the model for collision frequency:

$$C_{ij} = S_{ij}(u_{ti}^2 + u_{tj}^2)^{1/2}\eta_{ij} \tag{45}$$

The collision efficiency $\eta_{ij}$ is modeled by comparing the time required for coalescence $t_{ij}$ with the actual time during the collision $\tau_{ij}$:

$$\eta_{ij} = \exp(-t_{ij}/\tau_{ij}) \tag{46}$$

$$t_{ij} = \left(\frac{\rho_l r_{ij}^3}{16\sigma}\right)^{1/2} \ln\frac{h_0}{h_f} \tag{47}$$

$$\tau_{ij} = \frac{r_{ij}^{2/3}}{\varepsilon^{1/3}} \tag{48}$$

where $h_0$ is the initial film thickness, $h_f$ is the critical film thickness when rupture occurs, which are chosen as $1 \times 10^{-4}$ and $1 \times 10^{-8}$ m, respectively, and $r_{ij}$ is the equivalent radius:

$$r_{ij} = \left(\frac{1}{2}\left(\frac{1}{r_i} + \frac{1}{r_j}\right)\right)^{-1} \tag{49}$$

The cross-sectional area of the colliding is defined by:

$$S_{ij} = \frac{\pi}{4}(d_i + d_j)^2 \tag{50}$$

The turbulent velocity is given by:

$$u_{ti} = \sqrt{2}(\varepsilon d_i)^{1/3} \tag{51}$$

### *Initial and boundary conditions*

Transient calculations start from assuming that solid particles distribute uniformly in the reactor. The inlet gas velocities are determined according to the area of the distributor plate with the gas holdup of unity.

As $\frac{d_o^{1.5} U_{go} \rho_l g^{0.5}}{\sigma} \leq 1$ in our study (where $d_o$ is the diameter of the orifice and $U_{go}$ is the superficial gas velocity at the distribution plate), the size of bubbles produced at the orifice $d_b$ is calculated by[44]:

$$d_b = 2.9\left(\frac{\sigma d_o}{g\rho_l}\right)^{1/3} \tag{52}$$

The calculated result of the bubble diameter at the orifice $d_b = 4.48$ mm under the investigated experimental conditions, thus the size fraction of the third bubble group with the diameter of 4.5 mm is set to be unity for the inlet condition.

The boundary condition for the walls is defined as no-slip for the liquid phase and free-slip for the solid and the gas phases. At the top of the computational domain a proper outlet condition is defined so that only gas phase can leave the domain through the inner area, and only liquid phase can leave the domain through the periphery, whereas solid phase is kept within the reactor.[45]

### *Numerical solution*

The partial differential equations above are numerically solved using the commercial CFD code CFX. Unstructured grids of $10 \times 10 \times 15$ mm$^3$, $5 \times 10 \times 15$ mm$^3$ and $5 \times 5 \times 15$ mm$^3$ are implemented with a total number of 17,640 cells, with the mesh partition of the bottom and the column shown in Figure 1. To save the computing cost, a time-stepping strategy is used[46]: 100 steps at 0.001 s, 100 steps at 0.002 s, 100 steps at 0.005 s, 100 steps at 0.01 s, 100 steps at 0.02 s, 100 steps at 0.05 s, and for the rest time the time step length is 0.1 s. A typical solver run over 200 s of computed time (time averaging is carried out after 20 s for fully

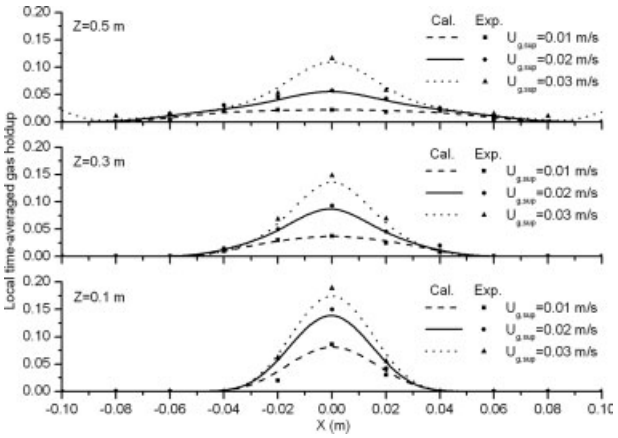


**Figure 2. Validation of model simulated local time-averaged gas holdups under different superficial gas velocities ($\varepsilon_{s,0}$ = 2%).**

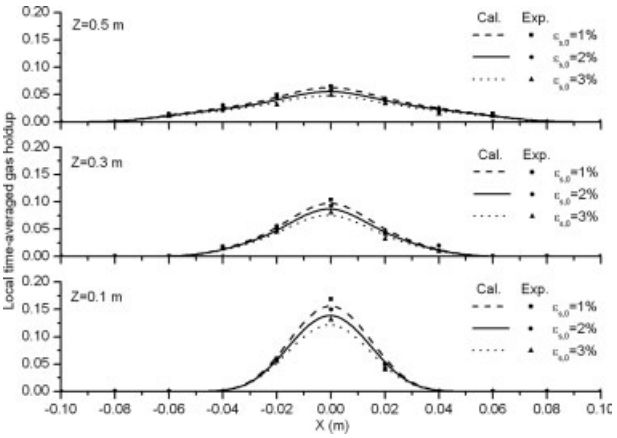


**Figure 3. Validation of model simulated local time-averaged gas holdups under different initial solid loadings ($U_{g,sup}$ = 0.02 m/s).**

fluidization) takes about 100 h on an Intel Pentium D 3.0 GHz processor. Convergence is good at the criteria of $1 \times 10^{-4}$ for all variables.

## Results and Discussion

### *Model simulation of local time-averaged gas holdups and axial liquid velocities*

Figure 2 is the comparison between the model simulated results and the experimental measured data of the local time-averaged gas holdups under different superficial gas velocities ($U_{g,sup}$ = 0.01, 0.02, 0.03 m/s) at different positions in the bubble column ($X$ = −0.1 to 0.1 m, $Y$ = 0 m, $Z$ = 0.1, 0.3, 0.5 m), and under the same initial solid loading of $\varepsilon_{s,0}$ = 2%. The experimental measurements agree very well with the model simulations with the correlation coefficients larger than 0.963 for all cases. It can be seen from this figure that the local time-averaged gas holdup at certain location increases with the increase in the superficial gas velocity. The central line of the reactor has higher local time-averaged gas holdups compared with the periphery of the reactor. With the rise in the axial position, the distribution of the local time-averaged gas holdups along the $x$-axis becomes flatter. However, it is interesting to notice that there is an obvious increase in the local time-averaged gas holdups at the periphery of the reactor at the axial position of $Z$ = 0.5 m, which is attributed to the recirculation of the gas bubbles brought by the downwards flowing liquid near the wall of the reactor.

Figure 3 shows the comparison between the model simulated results and the experimental measured data of the local time-averaged gas holdup under different initial solid loadings ($\varepsilon_{s,0}$ = 1, 2, 3%) at different positions in the bubble column ($X$ = −0.1 to 0.1 m, $Y$ = 0 m, $Z$ = 0.1, 0.3, 0.5 m), and under the fixed superficial gas velocity of $U_{g,sup}$ = 0.02 m/s. The agreements between the model simulations and the experimental measurements are very good as all the correlation coefficients are larger than 0.979. With the addition of the solid particles, the local time-averaged gas holdup at certain location decreases. However, it is clear that the effect of the changes in the initial solid loadings on the local time-averaged gas holdups shown in Figure 3 is smaller than that of the changes in the superficial gas velocities shown in Figure 2.

Figure 4 exhibits the comparison between the model simulated results and the LDA measured data of the local time-averaged axial liquid velocities under different superficial gas velocities ($U_{g,sup}$ = 0.01, 0.02, 0.03 m/s) at different positions in the bubble column ($X$ = −0.1 to 0.1 m, $Y$ = 0 m, $Z$ = 0.1, 0.3, 0.5 m), and under the same initial solid loading of $\varepsilon_{s,0}$ = 2%. The model predictions agree well with the LDA measurements as the correlation coefficients are larger than 0.991 for all situations. From this figure, it is obvious to see that the local time-averaged axial liquid velocity increases with the increase in the superficial gas velocities at certain location. Larger value of the local time-averaged axial liquid velocity occurs at the central line of the bubble column; whereas at the periphery of the reactor the direction of the local time-averaged axial liquid velocities is opposite because of the liquid recirculation as the result of the density

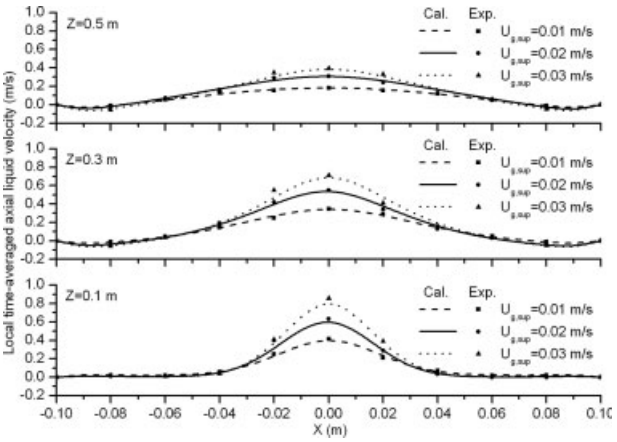


**Figure 4. Validation of model simulated local time-averaged axial liquid velocities under different superficial gas velocities ($\varepsilon_{s,0}$ = 2%).**

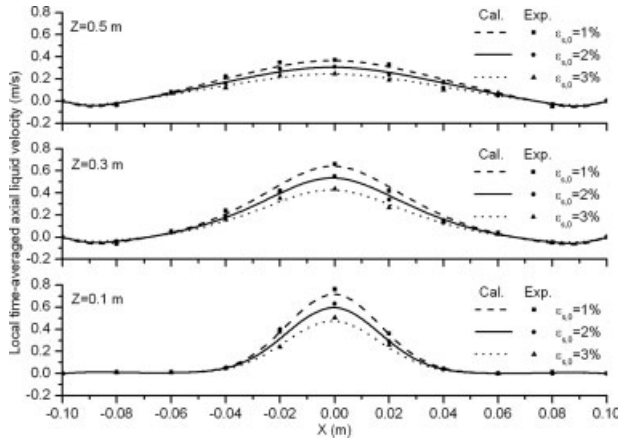


**Figure 5. Validation of model simulated local time-averaged axial liquid velocities under different initial solid loadings ($U_{g,sup}$ = 0.02 m/s).**

difference between the upper and the lower end of the reactor. The distribution profile of the local time-averaged axial liquid velocities along the $x$-axis is basically axial symmetry, which becomes much flatter as the increase in the axial position. However, the downwards local time-averaged axial liquid velocities at the periphery of the bubble column increase with the axial position.

The comparison between the model simulated results and the LDA measured data of the local time-averaged axial liquid velocities under different initial solid loadings ($\varepsilon_{s,0}$ = 1, 2, 3%) at different positions in the bubble column ($X$ = −0.1 to 0.1 m, $Y$ = 0 m, $Z$ = 0.1, 0.3, 0.5 m), and under the fixed superficial gas velocity of $U_{g,sup}$ = 0.02 m/s is illustrated in Figure 5. Good agreements between the model simulations and the experimental measurements are assured by the correlation coefficients larger than 0.986 for all cases. The increase in the initial solid loadings brings a negative effect on the local time-averaged axial liquid velocity as shown in the figure; a possible reason might be the reduced formation of fast-rising large bubbles in the presence of solids.

From Figures 2–5, it is clear that the agreements between the model simulated results and corresponding experimental measured data of local time-averaged gas holdup and axial liquid velocity profiles in the bubble column are very good, which should be contributed to the proper development of the CFD model and the application of the advanced experimental technologies. It is indicated that this developed CFD model can be adopted for simulating the time-averaged dynamic behaviors of the local hydrodynamic characteristics of the gas–liquid–solid three-phase bubble column.

### *Model prediction of local transient hydrodynamics*

As the measuring technology of the local transient dynamic behaviors of the whole reactor is rather limited, model predictions of the local transient hydrodynamics as well as the bubble size distribution are necessary for understanding and analysis of the factors, which may affect the multiphase reaction processes, such as liquid flow and mass transfer characteristics.

Figure 6 is the model prediction of the local transient hydrodynamic characteristics of the gas–liquid–solid three-phase bubble column under the fixed superficial gas velocity of $U_{g,sup}$ = 0.02 m/s and initial solid loading of $\varepsilon_{s,0}$ = 2% at the vertical section. The nine charts in Figure 6 show the model predicted local transient gas holdups, liquid velocities and solid holdups from up to down, and at different time of $t$ = 20, 110, 200 s from left to right, respectively. These charts visually exhibit the instantaneous dynamic behaviors of the local transient hydrodynamics of the three-phase bubble column. Gas bubbles are carried downward by the liquid circumfluence near the wall of the bubble column. A gas bubble plume is formed and moves wiggly in the reactor

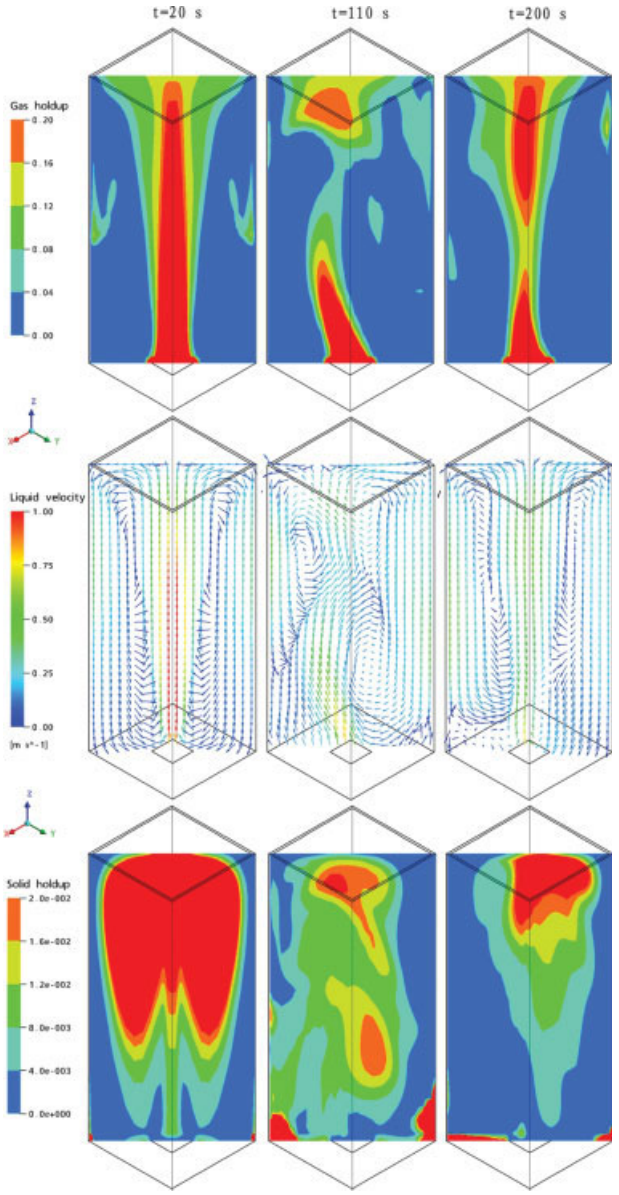


**Figure 6. Prediction of local transient hydrodynamic characteristics of the bubble column ($U_{g,sup}$ = 0.02 m/s and $\varepsilon_{s,0}$ = 2%).**

[Color figure can be viewed in the online issue, which is available at www.interscience.wiley.com.]

resulted from the interphase momentum transfer forces. Large vortices alongside the bubble plume are engendered, which further results in the nonuniform distribution of the solid particles within the reactor. It can be concluded from the figure that it is the pseudo-periodical wiggle of the gas bubble plume that originates the dynamic changes in the liquid velocities as well as the solid holdup distribution.

### *Model prediction of bubble size distribution*

In real bubble column multiphase reaction processes, the dispersion and interfacial heat- and mass-transfer fluxes, as well as the biochemical reaction rates, are closely related to the fluid dynamics of the system through the liquid–gas as well as liquid–solid contact area. Since the diameter of the solid particles is normally fixed, the dynamic changes of the bubble diameters will play an important role in the study of the multiphase reaction mechanisms. Then this developed CFD model is used to predict the transient dynamic behaviors of the bubble size distribution, which further can be used as a way to evaluate the momentum, heat and mass transfer performances between the gas–liquid and gas–solid interfaces of the gas–liquid–solid three-phase system in the bubble column.

Figure 7 is the model predicted bubble size distribution of the gas–liquid–solid three-phase bubble column under the fixed superficial gas velocity of $U_{g,sup}$ = 0.02 m/s and initial solid loading of $\varepsilon_{s,0}$ = 2% at the vertical section. The thirty charts within Figure 7 respectively illustrate the model predictions of the size fractions of the 10 bubble classes viz. Groups 1–10 at different time of $t$ = 20, 110, 200 s. Gas bubbles with the diameters ranging from 1 to 15 mm is divided into the 10 bubble classes, with the average diameter of each class is 1.7, 3.1, 4.5, 5.9, 7.3, 8.7, 10.1, 11.5, 12.9, 14.3 mm, respectively. It can be seen that small bubbles viz. bubble class Groups 1–5 prevail almost the whole reactor with size fractions mostly larger than 0.2; whereas large bubbles viz. bubble class Groups 6–10 have size fractions mostly smaller than 0.2. It should be noticed that there are locations with bubble class size fraction larger than 0.2 for Group 10 at $t$ = 20 s, which might be the result of sustaining bubble coalescence as the obvious gas recirculation there (refer to the chart of gas holdup prediction at $t$ = 20 s in Figure 6).

For better showing the bubble size distribution, the reactor volume-averaged bubble class size fractions of Groups 1–10 at $t$ = 20, 110, 200 s are calculated and shown in Figure 8. As obviously can be seen in this plot, the small bubbles of Groups 1–5 take a big part of all the gas bubbles (fraction sum $>$ 0.85); whereas large bubbles of Groups 6–10 take only a small part of all the gas bubbles (fraction sum $<$ 0.15), and the bubble size distribution is fluctuating with time changes. This may be attributed to the presence of solid particles of the multiphase flow, which indicates that the presence of solid particles may bring good effects on the gas–liquid mass transfer as the specific area of the bubbles increases. Further work on the CFD modeling of the real multiphase reaction processes coupling liquid flow, mass transfer, and intrinsic kinetics in the gas–liquid–solid three-phase bubble column is under way.

To better describe the benefits for considering bubble size distribution in modeling of the three-phase BC, simulation

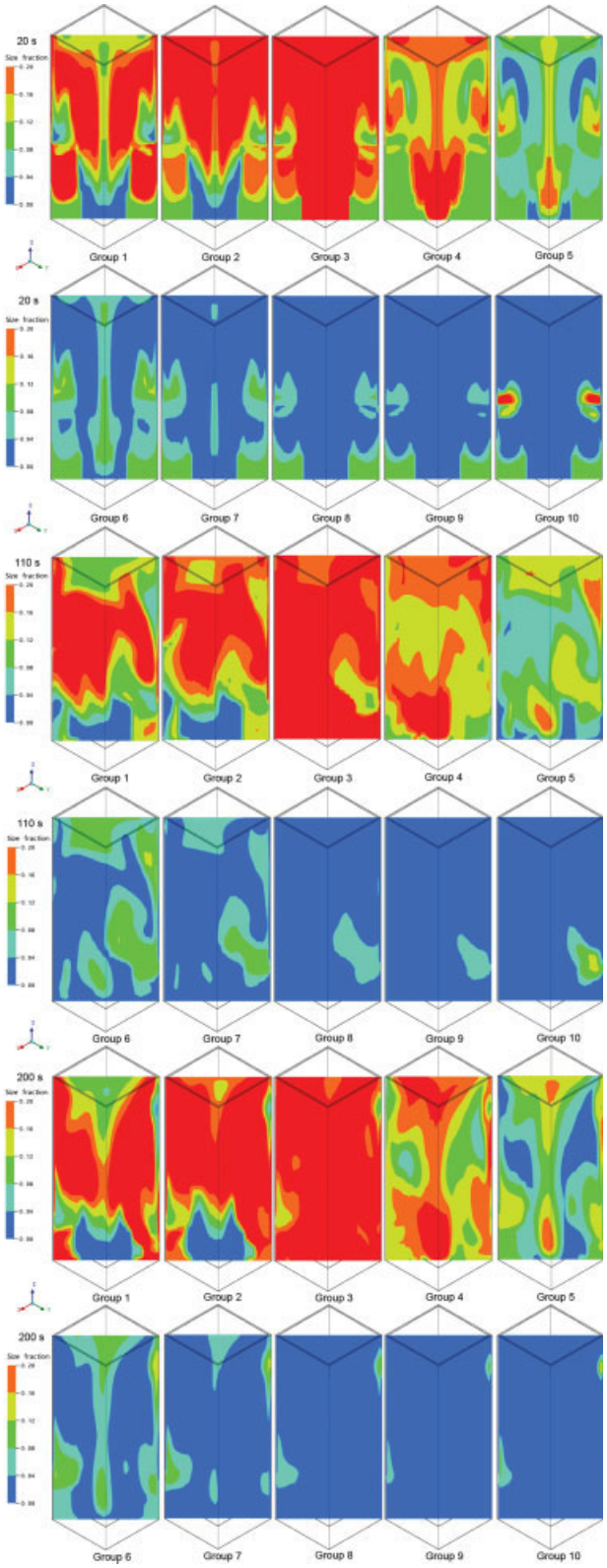


**Figure 7. Prediction of local transient bubble size distribution of the bubble column ($U_{g,sup}$ = 0.02 m/s and $\varepsilon_{s,0}$ = 2%).**

[Color figure can be viewed in the online issue, which is available at www.interscience.wiley.com.]

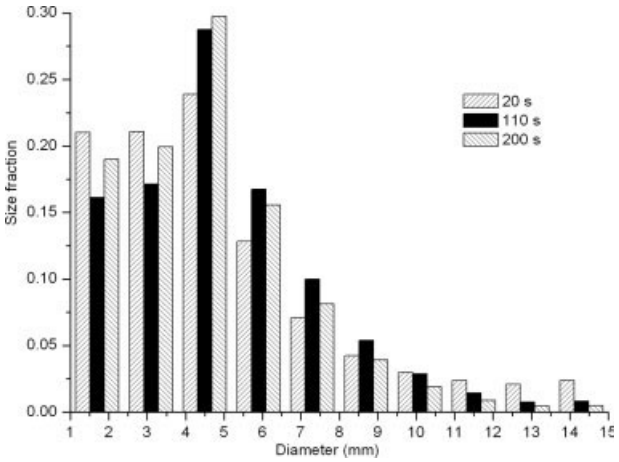


**Figure 8. Prediction of transient reactor volume-averaged bubble size distribution of the bubble column ($U_{g,sup}$ = 0.02 m/s and $\varepsilon_{s,0}$ = 2%).**

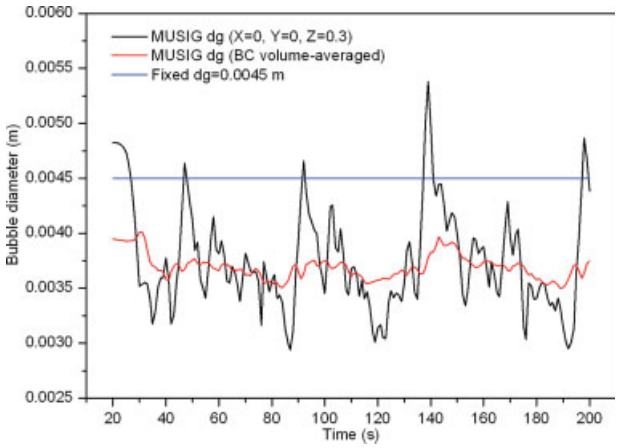


**Figure 9. Comparison of bubble diameter between simulations with bubble size distribution and fixed bubble diameter ($U_{g,sup}$ = 0.01 m/s and $\varepsilon_{s,0}$ = 2%).**

[Color figure can be viewed in the online issue, which is available at www.interscience.wiley.com.]

with fixed bubble diameter is performed under the operation condition of $U_{g,sup}$ = 0.01 m/s and $\varepsilon_{s,0}$ = 2%, and the results are compared with those of the simulation with bubble size distribution. According to Eq. 53, the inlet bubbles at the orifice of the reactor have a diameter of 4.48 mm under the investigated operating conditions, and then the third group of the bubbles with the diameter of 4.5 mm is chosen to be unity in the simulations with bubble size distribution. Thus the fixed bubble diameter is also set to be 4.5 mm for the current CFD simulation without considering bubble coalescence and breakup effects.

The simulation with fixed bubble diameter does not improve the convergence but saves much computation cost: it only takes about 50 h to complete the run, which is half of that with bubble size distribution, owing to the significant reduction of the number of PDEs. There are no obvious differences observed in the time-averaged and transient local hydrodynamics predicted by the two simulations (data not shown). It seems that the simulation with fixed bubble diameter is preferable for modeling of the local hydrodynamics of the three-phase BC, given the decent simulation results and the much lower computation cost.

However, from Figures 9 and 10 which show the comparison of the bubble diameter obtained from the simulations with bubble size distribution and with fixed bubble diameter, it is clear to see that the dynamic changes of the Sauter mean bubble diameter ($d_g$) at the local position, e.g., ($X$ = 0, $Y$ = 0, $Z$ = 0.3) is remarkable, corresponding to the fluctuating specific area ($a$) there; the BC volume-averaged Sauter mean bubble diameter is around 3.7 mm, which is much smaller than the 4.5 mm fixed bubble diameter, corresponding to the BC volume-averaged specific area of 1706.7 $m^{-1}$, which is much larger than the 1333.3 $m^{-1}$ fixed specific area. This difference makes the simulation with bubble size distribution much preferable in the calculation of the volumetric mass transfer coefficients ($K_l a$) and consequently the mass transfer rates and the bioreaction rates in the three-phase BC, which not only can better capture the real bioreaction rates in the whole reactor but also help one to better understand the distinct behaviors occur at any local positions in the reactor.

Based on the earlier discussion, the conclusion can be drawn then, that for modeling of the hydrodynamics only, simulation with fixed bubble diameter is preferable for saving the computation cost; whereas for modeling of the dynamic behaviors of the three-phase bioreaction process, simulation with bubble size distribution is necessary. This article deals with the fundamental work for modeling of the dynamic behaviors of the three-phase bioreaction process, thus population balance model must be adopted to consider the bubble size distribution.

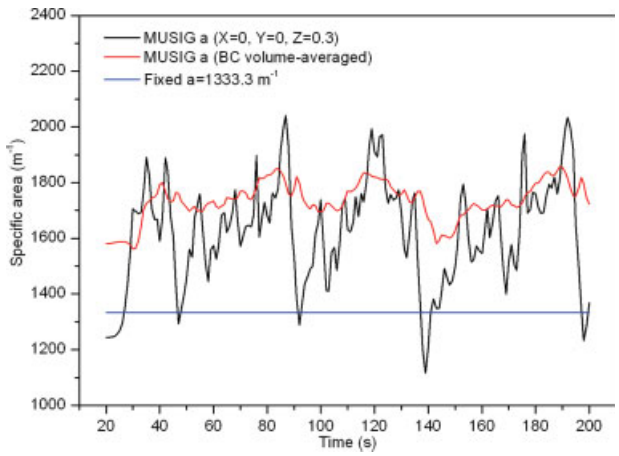


**Figure 10. Comparison of specific area between simulations with bubble size distribution and fixed bubble diameter ($U_{g,sup}$ = 0.01 m/s and $\varepsilon_{s,0}$ = 2%).**

[Color figure can be viewed in the online issue, which is available at www.interscience.wiley.com.]

## Conclusions

A 3-D transient CFD model for simulating the local hydrodynamics of a gas–liquid–solid three-phase bubble column reactor, with MUSIG model adopted to determine the size distribution of gas bubbles, was validated to be reliable by time-averaged data of the experimental measurements. Local transient hydrodynamics of the three-phase bubble column, such as gas holdups, solid holdups, liquid velocities, and bubble size distribution were also predicted reasonably by the developed model. The study on the dynamic behaviors of the bubble size may provide a useful method for understanding the mass transfer characteristics of the three-phase reaction in the bubble column.

This model is under improvement for simulating real three-phase reaction processes using immobilized microorganism, where three-phase liquid flow, interphase mass transfer and intrinsic kinetics should be coupled together. Moreover, this developed model can be further applied in many fields, such as to optimize the design and construction of the bubble column and the operation of the fermentation process, as well as to facilitate the scaleup strategies.

Detailed knowledge of the local fluid dynamics is very important in design and scaleup of the multiphase reactors. However, noninvasive optical techniques, such as LDA and particle imaging velocimetry, are restricted to characterizing velocity fields with low holdups of the dispersed phase. Thus nonoptical techniques, like computer-automated radioactive particle tracking, positron emission particle tracking, and computer-assisted tomography, may provide useful data for opaque systems at higher values of dispersed phase holdup,[47,48] which will be used in future study on the three-phase fermentation process.


## Acknowledgments

The authors wish to acknowledge the financial support provided by the Key National Natural Science Foundation of China (No. 20336030), Program for Science and Technology Development of Tianjin (No. 04318511120), Natural Science Foundation of Tianjin (No. 07JCZDJC01500), the Research Fund for the Doctoral Program of Higher Education (No. 20060056010), Program for New Century Excellent Talents in University, Program for Changjiang Scholars and Innovative Research Team in University, and Program of Introducing Talents of Discipline to Universities (No. B06006).


## Notation

$a$ = specific area, $m^{-1}$
$B$ = birth source, $kg/m^3$ s
$B_{ij}$ = specific breakup rate, 1/s
$C_B$ = constant, dimensionless
$C_D$ = drag coefficient, dimensionless
$C_{ij}$ = specific coalescence rate, $m^3/s$
$C_L$ = lift coefficient, dimensionless
$C_{\varepsilon 1}$ = constant, dimensionless
$C_{\varepsilon 2}$ = constant, dimensionless
$C_\mu$ = constant, dimensionless
$C_{\mu p}$ = constant, dimensionless
$D$ = death source, $kg/m^3$ s
$d$ = diameter, m
$E(\alpha_g)$ = correction term, dimensionless
Eo = Eotvos number, dimensionless
$f$ = size fraction, dimensionless
$f_{BV}$ = breakup fraction, dimensionless
$\mathbf{g}$ = gravitational acceleration, $m/s^2$
$h$ = film thickness, m
$K_la$ = volumetric mass transfer coefficient, $s^{-1}$
$k$ = turbulence kinetic energy, $m^2/s^2$
$\mathbf{M}_D$ = drag force, $N/m^3$
$\mathbf{M}_I$ = interphase momentum transfer force, $N/m^3$
$\mathbf{M}_L$ = lift force, $N/m^3$
$m$ = mass, kg
$n$ = number density, $1/m^3$
$P_k$ = turbulence production, kg/m $s^3$
$p$ = pressure, Pa
$Re$ = particle Reynolds number, dimensionless
$Re_m$ = mixture Reynolds number, dimensionless
$r_{ij}$ = equivalent radius, m
$S$ = source term, $kg/m^3$ s
$S_{ij}$ = cross-sectional area of the colliding, $m^2$
$t$ = time, s
$t_{ij}$ = time required for coalescence, s
$U_{go}$ = superficial gas velocity at the distribution plate, m/s
$\mathbf{u}$ = velocity vector, m/s
$u_t$ = turbulent velocity, m/s
$v$ = volume of bubbles, $m^3$
$X_{jki}$ = mass fraction, dimensionless

### *Greek letters*

$\alpha$ = volume fraction, dimensionless
$\beta$ = constant, dimensionless
$\varepsilon$ = turbulence eddy dissipation, $m^2/s^3$
$\eta_{ij}$ = collision efficiency, dimensionless
$\mu$ = molecular viscosity, Pa s
$\mu_{eff}$ = effective viscosity, Pa s
$\mu_{g,l}$ = gas particle induced viscosity of the liquid phase, Pa s
$\mu_{s,l}$ = solid particle induced viscosity of the liquid phase, Pa s
$\mu_T$ = turbulence induced viscosity, Pa s
$\rho$ = density, $kg/m^3$
$\sigma$ = surface tension, N/m
$\sigma_k$ = constant, dimensionless
$\sigma_\varepsilon$ = constant, dimensionless
$\tau$ = actual time during the collision, s
$\upsilon$ = kinematic viscosity, $m^2/s$
$\xi$ = dimensionless size of eddies in the inertial subrange of isotropic turbulence, dimensionless

### *Subscripts*

0 = initial condition
g = gas phase
$i$ = $i$th bubble group
$j$ = $j$th bubble group
$k$ = $k$th bubble group
l = liquid phase
o = orifice
s = solid phase
sup = superficial

## Literature Cited


1. Kantarci N, Borak F, Ulgen KO. Bubble column reactors. *Process Biochem*. 2005;40:2263–2283.
2. Jakobsen HA, Lindborg H, Dorao CA. Modeling of bubble column reactors: progress and limitations. *Ind Eng Chem Res*. 2005;44:5107–5151.
3. Monahan SM, Vitankar VS, Fox RO. CFD predictions for flow-regime transitions in bubble columns. *AIChE J*. 2005;51:1897–1923.
4. Delnoij E, Kuipers JAM, van Swaaij WPM. Computational fluid dynamics applied to gas–liquid contactors. *Chem Eng Sci*. 1997;52:3623–3638.
5. Lapin A, Lübbert A. Numerical simulation of the dynamics of two-phase gas–liquid flows in bubble columns reactors. *Chem Eng Sci*. 1994;49:3661–3674.
6. Sokolichin A, Eigenberger G. Gas–liquid flow in bubble columns and loop reactors, Part 1: detailed modeling and numerical simulation. *Chem Eng Sci*. 1994;49:5735–5746.

7. Sokolichin A, Eigenberger G, Lapin A, Lübbert A. Dynamic numerical simulation of gas–liquid two-phase flows: Euler/Euler versus Euler/Lagrange. *Chem Eng Sci*. 1997;52:611–626.
8. Pan Y, Dudukovic MP, Chang M. Numerical investigation of gas-driven flow in 2D bubble columns. *AIChE J*. 2000;46:434–449.
9. Chen P, Sanyal J, Dudukovic MP. CFD modeling of bubble columns flows: implementation of population balance. *Chem Eng Sci*. 2004; 59:5201–5207.
10. Hagesaether L, Jakobsen HA, Svendsen HF. Modeling of the dispersed-phase size distribution in bubble columns. *Ind Eng Chem Res*. 2002;41:2560–2570.
11. Lehr F, Mewes D. A transport equation for the interfacial area density applied to bubble columns. *Chem Eng Sci*. 2001;56:1159–1166.
12. Lehr F, Millies M, Mewes D. Bubble-size distributions and flow fields in bubble columns. *AIChE J*. 2002;48:2426–2443.
13. Sanyal J, Marchisio DL, Fox RO, Dhanasekharan K. On the comparison between population balance models for CFD simulation of bubble columns. *Ind Eng Chem Res*. 2005;44:5063–5072.
14. van den Hengel EIV, Deen NG, Kuipers JAM. Application of coalescence and breakup models in a discrete bubble model for bubble columns. *Ind Eng Chem Res*. 2005;44:5233–5245.
15. VBuwa VV, Ranade VV. Dynamics of gas–liquid flow in a rectangular bubble column: experiments and single/multi-group CFD simulations. *Chem Eng Sci*. 2002;57:4715–4736.
16. Olmos E, Gentric C, Vial C, Wild G, Midoux N. Numerical simulation of multiphase flow in bubble column reactors: influence of bubble coalescence and break-up. *Chem Eng Sci*. 2001;56:6359–6365.
17. Krishna R, van Baten JM, Urseanu MI. Three-phase Eulerian simulation of bubble column reactors operating in the churn-turbulent regime: a scale-up strategy. *Chem Eng Sci*. 2000;55:3275–3286.
18. Mudde RF, Simonin O. Two- and three-dimensional simulations of a bubble plume using a two-fluid model. *Chem Eng Sci*. 1999;54: 5061–5069.
19. Sanyal J, Vasquez S, Roy S, Dudukovic MP. Numerical simulation of gas–liquid dynamics in cylindrical bubble column reactors. *Chem Eng Sci*. 1999;54:5071–5083.
20. Sokolichin A, Eigenberger G. Applicability of the standard k-$\varepsilon$ turbulence model to the dynamic simulation of bubble columns, Part 1: detailed numerical simulations. *Chem Eng Sci*. 1999;54:2273–2284.
21. Delnoij E, Kuipers JAM, van Swaaij WPM. A three-dimensional CFD model for gas–liquid bubble columns. *Chem Eng Sci*. 1999;54: 2217–2226.
22. Pfleger D, Gomes S, Gilbert N, Wagner HG. Hydrodynamic simulations of laboratory scale bubble columns fundamental studies of the Eulerian-Eulerian modelling approach. *Chem Eng Sci*. 1999;54: 5091–5099.
23. Ranade VV, Tayalia Y. Modelling of fluid dynamics and mixing in shallow bubble column reactors: influence of sparger design. *Chem Eng Sci*. 2001;56:1667–1675.
24. Deen NG, van SintAnnaland M, Kuipers JAM. Multi-scale modeling of dispersed gas–liquid two-phase flow. *Chem Eng Sci*. 2004;59: 1853–1861.
25. Delnoij E, Lammers FA, Kuipers JAM, van Swaaij WPM. Dynamic simulation of dispersed gas–iquid two-phase flow using a discrete bubble model. *Chem Eng Sci*. 1997;52:1429–1458.
26. Ekambara K, Dhotre MT, Joshi JB. CFD simulations of bubble column reactors: 1D, 2D and 3D approach. *Chem Eng Sci*. 2005;60: 6733–6746.
27. Krishna R, van Baten JM. Eulerian simulations of bubble columns operating at elevated pressures in the churn turbulent flow regime. *Chem Eng Sci*. 2001;56:6249–6258.
28. Pfeger D, Becker S. Modelling and simulation of the dynamic flow behavior in a bubble column. *Chem Eng Sci*. 2001;56:1737–1747.
29. Spicka P, Dias MM, Lopes JCB. Gas–liquid flow in a 2D column: Comparison between experimental data and CFD modeling. *Chem Eng Sci*. 2001;56:6367–6383.
30. Thakre SS, Joshi JB. CFD simulation of bubble column reactors: importance of drag force formulation. *Chem Eng Sci*. 1999;54:5055–5060.
31. Vitankar VS, Dhotre MT, Joshi JB. A low Reynolds number k-$\varepsilon$ model for the prediction of flow pattern and pressure drop in bubble column reactors. *Chem Eng Sci*. 2002;57:3235–3250.
32. Michele V, Hempel DC. Liquid flow and phase holdup-measurement and CFD modeling for two-and three-phase bubble columns. *Chem Eng Sci*. 2002;57:1899–1908.
33. Cartland Glover GM, Generalis SC. Gas–liquid–solid flow modelling in a bubble column. *Chem Eng Process*. 2004;43:117–126.
34. Zhang XY, Ahmadi G. Eulerian-Lagrangian simulations of liquid–gas–solid flows in three-phase slurry reactors. *Chem Eng Sci*. 2005; 60:5089–5104.
35. Feng W, Wen JP, Fan JH, Yuan Q, Jia XQ, Sun Y. Local hydrodynamics of gas–liquid-nanoparticles three-phase fluidization. *Chem Eng Sci*. 2005;60:6887–6898.
36. Cui Z, Fan LS. Turbulence energy distributions in bubbling gas–liquid and gas–liquid–solid flow systems. *Chem Eng Sci*. 2004;59: 1755–1766.
37. Ishii M, Zuber N. Drag coefficient and relative velocity in bubbly, droplet or particulate flows. *AIChE J*. 1979;25:843–855.
38. Wen CY, Yu YH. Mechanics of fluidization. *Chem Eng Prog*. 1966; 62:100–111.
39. Sato Y, Sekoguchi K. Liquid velocity distribution in two-phase bubbly flow. *Int J Multiphase Flow*. 1975;2:79–95.
40. Schallenberg J, Enß JH, Hempel DC. The important role of local dispersed phase hold-ups for the calculation of three-phase bubble columns. *Chem Eng Sci*. 2005;60:6027–6033.
41. Olmos E, Gentric C, Midoux N. Numerical description of flow regime transitions in bubble column reactors by a multiple gas phase model. *Chem Eng Sci*. 2003;58:2113–2121.
42. Luo SM, Svendsen H. Theoretical model for drop and bubble breakup in rurbulent dispersions. *AIChE J*. 1996;42:1225–1233.
43. Prince M, Blanch H. Bubble coalescence and break-up in air-sparged bubble columns. *AIChE J*. 1990;36:1485–1499.
44. Chen P, Dudukovic MP, Sanyal J. Three-dimensional simulation of bubble column flows with bubble coalescence and breakup. *AIChE J*. 2005;51:696–712.
45. Padial NT, VanderHeyden WB, Rauenzahn RM, Yarbro SL. Three-dimensional simulation of a three-phase draft-tube bubble column. *Chem Eng Sci*. 2000;55:3261–3273.
46. Krishna R, van Baten JM, Urseanu MI, Ellenberger J. Design and scale up of a bubble column slurryreactor for Fisch-Tropsch synthesis. *Chem Eng Sci*. 2001;56:537–545.
47. Rammohan AR, Dudukovic MP, Ranade VV. Eulerian flow field estimation from particle trajectories: numerical experiments for stirred tank type flows. *Ind Eng Chem Res*. 2003;42:2589–2601.
48. Khopkar AR, Rammohan AR, Ranade VV, Dudukovic MP. Gas–liquid flow generated by a Rushton turbine in stirred vessel: CARPT/CT measurements and CFD simulations. *Chem Eng Sci*. 2005; 60:2215–2229.

*Manuscript received Oct. 26, 2006, and revision received Jun. 12, 2007.*